THE MEASUREMENT OF FLUID VELOCITIES IN POROUS MEDIA

Carl M. Edwards, Chii-Tzong Chang, and Subhendra Sarkar
Engineering Imaging Laboratory
Texas A&M University
College Station, Texas

ABSTRACT

NMR imaging techniques can provide spatial information about matrix porosity and about fluid saturations during multiphase flow. The most powerful feature of NMR imaging is the variety of contrast schemes available. These include relaxation time contrast, chemical shift separation, and phase shifts induced by molecular motion in pulsed field gradient (PFG) experiments. Relaxation and PFG diffusion measurements provide information concerning the microscopic structure of the porous matrix. Important as these measurements are, they provide direct information about the way fluids are *stored* but only indirect information about the way fluids are *transported.*

PFG techniques can also be used to directly measure properties of the coherent motion of fluids in porous media. We have applied these methods to measure both the spatial dependence of components of the average fluid velocity, $\langle V \rangle$, and the velocity distribution function, n(v). Both $\langle V \rangle$ and n(v) data were obtained using a stimulated echo pulse sequence because it has significant advantages for measuring slow flow. $\langle V \rangle$ is proportional to the permeability of the porous media, and thus provides a direct measurement of fluid transport. It is measured by inducing a phase shift, ϕ, in the NMR signal. Estimates of $\langle V \rangle$ using this method depend in a complicated way on the magnitude of the induced phase, the strength of the applied gradient, and the measurement time. Because the pores are much smaller than image resolution, the width of n(v) for each pixel is the same order of magnitude as $\langle V \rangle$. $|\phi| << 1$ for $\phi \propto \langle V \rangle G$.

Measurements of n(v) projected along the flow axis have also been performed. When the magnetic field gradient is applied parallel to the net flow, n(v) depicts the dynamic displacement profile for flow superimposed on diffusion. We have found that n(v) is affected by the observation time and diffusion of fluid molecules both perpendicular and parallel to flow streamlines is responsible.

INTRODUCTION

In recent years, the development of CT X-ray and nuclear magnetic resonance imaging (MRI) methods have provided unprecedented means for determining information corresponding to local regions within porous media. Much of the work to date has been directed to characterizing the porosity and fluid saturations. While this information provides important data about the manner in which the fluids are *stored,* it provides little information about how the fluids are *transported.* Such information is critical for developing a better understanding of how fluids are displaced in heterogeneous media.

NMR imaging methods can be extended to the measurement of fluid velocity. Recently work has yielded spatial maps of the average fluid velocity within each voxel. [1,2,3,4,5] Distribution functions of fluid velocities within a volume have also been measured.[5,6] These measurements are dynamic rather than static in nature and provide information about the mechanisms of fluid transport. The interpretation of these measurements has been rudimentary despite this recent flurry of work .

A number of different flow parameters might be characterized by these measurements. Average fluid velocity is proportional to the rock permeability. Even though the pressure gradient is unmeasurable on a millimeter scale, it may be possible produce a three dimensional map of permeability in a rock sample using estimation procedures.[7] Velocity distribution functions depend on pore space geometry in a complex way. Nevertheless it may be possible to extract meaningful geometrical information from these distribution functions such as fraction of flowing and nonflowing fluid.

To develop proper interpretations of the NMR measurements great care needs to be taken. The narrow pulse approximation must be valid and the role of a finite velocity observation time must correctly ascertained. We have found that naive assumptions about the measurement process may lead to incorrect characterization of the flow process. In the remainder of this paper we discuss the NMR velocity measurement processes, the steps required to obtain reliable data, and the pitfalls which are present in utilizing the data to describe fluid flow in porous media.

METHODOLOGY

The method we use to perform velocity imaging utilizes two gradient pulses of duration δ and magnitude G which are separated by time period Δ. This portion of the pulse sequence is shown in fig. 1. The sequence shown uses a stimulated echo to detect the NMR signal. The initial 90° RF pulse excites the transverse magnetization and the first gradient pulse encodes the position of every molecule in the phase of its transverse magnetization. The second 90° pulse stores the transverse magnetization along the static magnetic field while the third 90° pulse restores the magnetization to the transverse plane to be detected as the stimulated echo. The second gradient pulse is identical in area to the first. If the molecules have not moved during Δ, this pulse removes the phase encoded position information from the magnetization. For molecules which have moved there is a net change in phase in it's transverse magnetization caused either by coherent or incoherent molecular motion projected along the direction of the gradient (the z direction). If the gradient pulses are sufficiently short, the phase change is given by

$$\phi = \gamma G \delta (z(t) - z(t+\Delta)) = (\gamma G \delta \Delta) v. \tag{1}$$

The phase shift is proportional to the velocity, v, if each molecule has a definite velocity. Inducing a phase shift is one of a variety of ways to image fluid velocities.

This method, phase encoded velocity imaging, works equally well using either a Hahn spin echo pulse sequence or a stimulated echo sequence. The minimum detectable velocity, v_{min}, for the stimulated echo sequence is given by[8]

$$\phi_{min} = \gamma G_{max} T_2 T_1 v_{min}. \tag{2}$$

The value of ϕ_{min} depends on the quantity being measured. For velocity distributions, $\phi_{min} = \pi$. For average velocity measurements the actual value of ϕ_{min} depends on the signal-to-noise ratio but is usually much less than 1. In a Hahn spin echo sequence T_1 is replaced by T_2 in expression 2. The stimulated echo method is much more sensitive because $T_1 >> T_2$ for fluids to porous media,. We utilize this method in order to use small fluid flow rates.

The presence of the porous matrix has a profound effect on the velocity measurement process. For bulk fluids all molecules within the volume of interest (voxel) have velocities which are uniform and the width of

the velocity distribution function is narrow compared to its first moment. Any voxel size within experimental reach contains many pores for most porous media of interest in oil production. Single pores are generally not resolvable. For laminar flow, the molecular velocity is 0 in the pore/fluid boundary layer and reaches a maximum velocity in the center of the pore throats. The width of the velocity spectrum may be of the same order as the first moment. As an example, one can consider flow in bundled capillary tubes. In this case, the full width at half maximum of the velocity spectrum is exactly twice as large as its first moment.

During the observation time, Δ, a significant number of molecules may be displaced a distance comparable the characteristic pore size. These molecules will have a time varying velocity. Depending on the pore throat to radius ratio, the magnitude of this variation could also be of the same order as the first moment of the velocity spectrum. The effect of a finite observation time will be to average each molecule's velocity.

One final effect to consider is molecular diffusion. Molecules will diffuse a distance $\sqrt{6D\Delta}$ during Δ, with D equal to the fluid's self-diffusion constant. If this distance is comparable to a pore radius, molecules will diffuse across velocity streamlines. The effect of the diffusion process will be an additional averaging of each molecule's velocity.

The description of the fluid flow process can be summarized as follows. Within the porous structure the fluid is undergoing laminar flow. Because each voxel contains many pores, the instantaneous velocity spectrum will have components at $v = 0$ and at velocities considerably larger than the average fluid velocity $\langle V \rangle$. The effect of the finite observation time will be to average molecular velocities because of spatial and temporal variations. In order to properly interpret the NMR velocity measurements, the analysis of the data must explicitly consider these effects.

The starting point of the analysis is the conditional probability, $P(\mathbf{r} \mid \mathbf{r}'; t)$. $P(\mathbf{r} \mid \mathbf{r}'; t)$ is the probability of that a molecule initially at $\mathbf{r}$ will be at $\mathbf{r}'$ at a time t. In the narrow pulse approximation, the echo amplitude is given by[9]

$$E(q,\Delta) = \int dz\, \rho(z) \int dz'\, P(z \mid z'; \Delta) \exp\{iq \cdot (z' - z)\}, \tag{3}$$

where $q = \gamma G \delta$. In this equation we have integrated over all coordinates except for those in the direction of the magnetic field gradient. The narrow pulse approximation assumes that motion of fluid molecules during encoding and decoding gradient pulses is unimportant. To the extent that this approximation is valid, the analysis of the NMR experiment is analogous to analysis neutron scattering experiments.[9]

Callaghan[9] defines the averaged propagator as

$$\bar{P}(\zeta;\Delta) = \int dz\, \rho(z)\, P(z \mid z + \zeta; \Delta). \tag{4}$$

It is the probability that a molecule has moved a distance ζ during Δ. The echo intensity can be recast in term of $\bar{P}$.

$$E(q,\Delta) = \int d\zeta\, \bar{P}(\zeta; \Delta) \exp\{iq \cdot \zeta\}. \tag{5}$$

From eqn. 5 it is apparent that the Fourier transform of $E(q,\Delta)$ is $\bar{P}(\zeta;\Delta)$. Thus when a velocity imaging experiment is performed, the result of a velocity imaging experiment is not a velocity spectrum, but rather the averaged propagator. This is a statistical measure of the fluid displacement process. It measures the fraction of molecules that have been displaced a distance ζ.

It is possible to obtain a "velocity" distribution function from the averaged propagator. An average velocity can be defined as $\bar{v} = \zeta/\Delta$. $\bar{v}$ is the time average of each molecule's velocity.

$$\bar{v}(\Delta) = \frac{1}{\Delta}\int_{t}^{t+\Delta} dt'\, v(t'). \tag{6}$$

It is a property of each molecule. The velocity distribution function represents the fraction of molecules in the fluid with $\bar{v}$ and is then given by

$$n(\bar{v};\Delta) = \bar{P}(\zeta;\Delta)\left|\frac{d\bar{v}}{d\zeta}\right|^{-1}. \tag{7}$$

Several properties of $n(\bar{v};\Delta)$ will be useful to know in order to interpret the results of velocity measurements in porous media. For small Δ, velocity of each molecule will undergo little averaging and $n(\bar{v};\Delta)$ will approach the instantaneous velocity spectrum with a component at a maximum velocity corresponding to fluid in the center of the pore throats and a component at $v = 0$ corresponding to the pore/fluid boundary layer. At large Δ each molecule's $\bar{v}$ will approach the average fluid velocity as defined by Darcy's law and

$$\lim_{\Delta \to \infty} n(\bar{v};\Delta) = \delta(\bar{v} - \langle V \rangle). \tag{8}$$

The first moment of $n(\bar{v};\Delta)$ is the average fluid velocity. We denote it by $\langle V \rangle$. The bracket indicates it is an ensemble average rather than a time average. It is capitalized to indicate it is a macroscopic rather than a microscopic quantity.

$$\langle V \rangle = \int d\bar{v}\, \bar{v}\, n(\bar{v};\Delta). \tag{9}$$

From physical reasoning, $\langle V \rangle$ is independent of Δ and this requires that

$$\frac{d}{dt}\bar{v}\, n(\bar{v};t) = 0. \tag{10}$$

Having examined the methodology associated with the measurement of $n(\bar{v};\Delta)$, we now turn to the measurement process involved in directly measuring $\langle V \rangle$. Instead of Fourier transforming the $E(q,\Delta)$ with respect to $q\Delta$, the phase of $E(q,\Delta)$ is measured for small values of $q\Delta$. Under certain conditions, the phase of $E(q,\Delta)$ is proportional to $\langle V \rangle$. To understand why this is so and to understand what the appropriate conditions are, we begin by rewriting eqn. 3.

$$E(q,\Delta) = \int n(\bar{v};\Delta)\, \exp\{iq\Delta\bar{v}\}\, d\bar{v}. \tag{11}$$

In terms of the average velocity $\langle V\rangle$ for the voxel:

$$E(q,\Delta) = \exp\{iq\Delta\langle V\rangle\} \int n(\bar{v};\Delta)\exp\{iq\Delta(\bar{v} - \langle V\rangle)\}d\bar{v}. \tag{12}$$

If the integral in eqn. 12 is real, then the phase of the signal is given by $\phi = q\Delta\langle V\rangle$. ϕ is proportional to $\langle V\rangle$. For the integral to be real, $n(\bar{v};\Delta)$ must be symmetric about $\langle V\rangle$. This is generally not true for flow through porous media. However, if an appropriate pulsed gradient is employed so that the following condition is satisfied:[10]

$$q\Delta(\bar{v} - \langle V\rangle) << 1, \tag{13}$$

for all values of $\bar{v}$ where $n(\bar{v};\Delta) \neq 0$, then the phase of the NMR signal in eqn.. 12 can be approximated by

$$\phi \approx q\Delta\langle V\rangle. \tag{14}$$

The average velocity can then be estimated from ϕ. The accuracy of this approximation depends on the magnitude of the first moment of the gradient as well as the velocity spread in a voxel.

RESULTS

The instrumentation used for this project is a General Electric 2T/31 CSI system operating at a proton resonance frequency of 85.5 MHz. Magnetic field gradients were provided by a shielded gradient set with 200 μsec settling time. A 4.3 cm i.d. birdcage RF probe was used for both radiofrequency transmission and reception of the NMR signal. We performed a series of velocity imaging experiments on single phase fluid flow through a Bentheim sandstone sample and unconsolidated beadpacks. Sample characteristics are shown in table 1 and the parameters for NMR measurements are shown in table 2.

Table 1. Physical Properties of the Samples

	Beadpack	Bentheim
Diameter (mm)	20	25.4
Length (mm)	75	47
Porosity	0.38	0.23

Fig. 2 shows the velocity distribution functions of water flow (16 ml/min) in the 0.2 mm beadpack. Three sets of data were obtained at observation times of 0.1, 0.3 and 0.75 sec with the gradient in the direction of flow. The data represents the $n(\bar{v};\Delta)$ along the direction of flow. At an observation time of 0.3 sec, $n(\bar{v};\Delta)$ has a significant component at zero velocity, is not symmetric, and has the largest width of all three data sets. As the observation time is increased, the component at zero velocity disappears, the width decreases and the distribution becomes more symmetric.

The velocity distribution function of water flow at 4.8 ml/min through the Bentheim sample is shown in Fig. 3. $n(\bar{v};\Delta)$ was measured at observation times of 0.3, 0.5, and 0.75 sec. It has a significant component

at zero velocity at all observation times and a small nonzero values at velocities up to 2 mm/sec. Even with the significant change in Δ, $n(\bar{v};\Delta)$ changes little over the range of observation times.

Table 2. Velocity Imaging Parameters

	Beadpack	Bentheim
Recycle Time (s)	6.5	5.5
Image resolution	64 x 64	64 x 64
Field of View (mm)	71.42	71.42
Slice Thickness (mm)	5	5
Echo Time (ms)	8	8
Number of Average	16	16

The average velocity images were obtained by performing NMR imaging experiments for different values of the gradient amplitude and calculating the velocity by a voxel-by-voxel linear regression of the signal phase. Figs. 4 and 5 are the cross-section velocity images of water flow in the 0.2 mm beadpack and the Bentheim sample, respectively. The flow rates were 1.5 ml/min in Fig..4 and 2.0 ml/min in Fig. 5. We can also estimate the flow velocity from the volume flow rate to get an idea of the velocity measurement accuracy. Fig. 4 gives an average velocity of 0.21 mm/s over the cross sectional area, which is in good agreement with the Dupuit-Forchheimer velocity.[11] For the Bentheim sample the velocity image yields an average velocity of 0.19 mm/s. This number is smaller than the Dupuit-Forchheimer velocity by 30%.

DISCUSSION

$n(\bar{v};\Delta)$ is derived from the averaged propagator. $\bar{P}(\zeta,\Delta)$ is the conditional probability for a displacement ζ, averaged over initial positions. The conditional probability satisfies the following equation with appropriate boundary conditions.[9]

$$\frac{\partial P}{\partial t} = D\,\nabla^2 P + \vec{\nabla}\cdot(\vec{v}\,P). \tag{15}$$

The first term on the right hand side of equation 15 accounts for the effects of self-diffusion. The second term accounts for potential flow. This equation is difficult to solve when the boundary conditions appropriate to flow in porous media are imposed. Without the diffusion term, the solution of equation 15 will yield n(v;0). To correctly interpret the NMR velocity measurements we need to determine under what conditions the diffusion term can safely be ignored.

Fig. 6 shows the projection of a typical path a molecule might take in a capillary tube while undergoing diffusion and flow. The path is projected on a plane perpendicular to the capillary's cylindrical axis. The gray background represents the fluid velocity along the capillary. It is maximum at the center of the capillary and 0 at the walls. In this Fig. the radius of the capillary tube is 45 μm and the molecule's path is observed for approximately 0.5 seconds. The time interval and capillary radius were chosen to be typical of the applications of velocity imaging techniques to flow in porous media. During this time interval, the molecule samples many different regions of the capillary cross-section and therefore samples many different velocity streamlines. Thus the molecule's displacement along the direction of flow is not well represented by the velocity of a single streamline. It is rather the average of many different streamlines.

We performed a number of computer simulations of flow between parallel flat plates to observe the effect the diffusion term in equation 15 on the measurement of $n(\bar{v};\Delta)$. Flow between flat plates was chosen as the

initial configuration for our simulations because the boundary conditions are simple to impose. Particles were started along a line perpendicular to the flow direction. They were permitted to random walk in both directions with a probability of 0.25 for taking a positive or negative step and 0.5 for remaining stationary. At each time interval the particles were also displaced because of the bulk fluid velocity. The time interval, τ, between steps was chosen so that $2D\tau << a^2$ and the step length is $\sqrt{2D\tau}$. 2a is the spacing between the plates. D was taken to 2000 μm^2/sec, approximately the self-diffusion coefficient of water at room temperature. The iterative equations used in the simulations were

$$\begin{aligned} x_{i+1} &= x_i + x_r + v_m\left(1 - \frac{y_i^2}{a^2}\right)\tau, \\ y_{i+1} &= y_i + y_r, \\ x_r, y_r &= 0, \pm\sqrt{2D\tau}. \end{aligned} \tag{16}$$

The r subscript indicates the random step. v_m is the fluid velocity at the center of the capillary. The displacement of each particle was sampled at intervals corresponding to typical observation times. At each of these observation times a histogram was calculated as the path of each particle was determined. This histogram corresponds to the averaged propagator. Each simulation was run with 40,000 or 80,000 particles. The distance between the plates was varied for each different simulation. At the end of the simulation the averaged propagator was used to calculate the $n(\bar{v};\Delta)$ according to eqn. 7.

Fig. 7 are the results of one such simulation. $n(\bar{v};\Delta)$ for a number of different observation times in the range of 5 msec to 1 sec. v_m is 8.9 mm/sec and a = 45 μm. The range of observation times and the inter-plate spacing were chosen to be "typical" for porous media. v_m was chosen to be large in order to illustrate the effect of diffusion perpendicular to flow. The analytical result without the diffusion term is also shown. The analytical result is not well reproduced by the simulation except at small observation times. As Δ increases, $n(\bar{v};\Delta)$ becomes more narrow. Furthermore, the first moment of the distribution, $\langle V \rangle$ is independent of Δ and is equal to the $\langle V \rangle$ calculated from the analytical result. This dependence on Δ is similar to the behavior of $n(\bar{v};\Delta)$ for the glass beadpack shown in fig. 2.

Fig. 8 shows the results from a simulation with v_m = 0.89 mm/sec. In this simulation, $n(\bar{v};\Delta)$ never accurately reproduces the analytical calculation. At small observation times, $n(\bar{v};\Delta)$ is much broader than the analytical calculation and a significant fraction of the molecules exhibit negative displacements. This is the result of diffusion along the direction of flow.

Figs. 7 and 8 illustrate the upper and lower limits of the observation time. The upper limit requires that the molecules do not sample an appreciable number of velocity streamlines during the observation time. Thus the distance a molecule diffuses must be much less than the characteristic size of the pore. That is

$$\sqrt{2D\Delta} << a, \text{ or } \Delta << \frac{a^2}{2D}. \tag{17}$$

As this limit is exceeded, the molecules sample more and more velocity streamlines and $n(\bar{v};\Delta)$ will approach $\delta(\bar{v} - \langle V \rangle)$. This limit is sensitive to the square of the characteristic pore length. It will be difficult to satisfy for materials with small pores using ordinary NMR instrumentation for materials with small pores.

The lower limit requires that the distance a molecule diffuses is much less than the distance the molecule is displaced due to coherent motion.

$$\sqrt{2D\Delta} << v_m\Delta, \text{ or } \Delta >> \frac{2D}{v_m^2}. \tag{18}$$

As Δ is made smaller than this limit, $n(\bar{v};\Delta)$ will become more and more gaussian reflecting the importance of the diffusion process parallel to flow. This limit is inversely proportional to the characteristic pore velocity and is difficult to satisfy for reservoir flow rates.

An accurate estimate of n(v;0) seems impossible to obtain. However there is hope. The lower limit is proportional to the diffusion constant, while the upper limit is inversely proportional to D. If a more viscous fluid is used in the measurement, then it will be easier to estimate n(v;0). Fig. 9 is a comparison of $n(\bar{v};\Delta)$ for water and Soltrol-130 flowing through the 0.2 mm beadpack at a flow rate of 5 ml/min. The observation time was 0.5 sec. Since Soltrol-130 has a molecular diffusion rate of about one third of that of water, we would expect that the Soltrol-130 result would resemble the water result with a shorter observation time. Indeed, the Soltrol result has a larger width than the water result at Δ = 0.5 sec. Comparison with Fig. 2 indicates that the Soltrol result is similar to the water result at Δ = 0.1 sec.

The velocity spectrum for water flow in Bentheim sandstone (fig. 3) indicates that much of the water is either stagnant or very slowly moving. This spectrum changes little over the range of observation times used in the study. This indicates that the stagnant fluid is at least 50 μm (> $\sqrt{2D\Delta}$) removed from flowing channels. The stagnant fluid could be in nonflowing pores or in nonflowing regions of flowing pores.[12] Our present measurements do not distinguish these two contributions. If the flow rate through the sample was increased enough to give all the fluid in flowing pores a measurable velocity, only the fluid in nonflowing pores would remain stagnant and the two components could be distinguished.

The small tail to the Bentheim spectrum is also an important feature. Because fluid velocities will be largest in the pore throats, this tail could results from molecules moving through the throats. If this identification is valid, approximated 25% of the fluid flowed through pore throats during the observation time.

We now turn to the examination of $\langle V \rangle$ images. As seen from eqn. 12, $n(\bar{v};\Delta)$ plays an important role in the behavior of the net phase shift. Fig. 10 shows the phase shift as a function of $q\Delta$ from an image voxel for water flow (1.6 ml/min) in the 0.2 mm beadpack. It is apparent that the data obtained with the shorter observation time deviate from the linearity earlier as $q\Delta$ is increased. This is consistent with the $n(\bar{v};\Delta)$ measurements which indicate a broader $n(\bar{v};\Delta)$ for the shorter Δ. Therefore, special care must be exercised in order to obtain a reliable measurement of the average velocity from the phase shift of an image voxel. One must be certain that eqn. 13 is well satisfied for all $\bar{v}$ where $n(\bar{v},\Delta) \neq 0$.

Fig. 11 compares the results of the finite pulse and the narrow pulse experiments. It shows the phase shift as a function of the first moment of the gradient for water flow (2 ml/min) through the Bentheim sample. Four different PFG time scales were used for which the first two satisfy the narrow-pulse condition whereas the last two do not. For each PFG time scale, the phase shift was measured with different values of gradient amplitude. The significance of this result is that, while the phase shift is linearly proportional to the first moment of the gradient for all data sets, only for the case of narrow pulses is its slope independent of the observation time. In other words, under the narrow pulse condition a unique value of average

velocity independent of the observation time can be determined. On the contrary, in the finite pulse case the phase shift is not related to the average velocity in a simple way.

If Darcy's law is satisfied, the fluid velocity at each voxel is expected to be proportional to the flow rate. The effect of changing the flow rate on the phase shift is shown in Figs. 12 and 13. The phase shift of water flow in the Bentheim sample normalized to the flow rate is plotted against the gradient amplitude. Fig. 12 shows that at small gradient amplitudes (< 3 G/cm) where the condition in eqn. 13 is satisfied, the phase shift is linearly proportional to the gradient amplitude and the average velocity can be derived from the slope. Moreover, the average velocity so determined is proportional to the flow rate. In fig. 13, which was obtained from the finite-pulse experiments, and the phase shift is not proportional to the flow rate.

CONCLUSIONS

We have been able to produce spatial maps of $\langle V \rangle$ in simple porous systems. In order to obtain reliable data, the net phase shift caused by coherent motion must be small. Furthermore by increasing the observation time the regime where $\phi \propto q\Delta$ is increased. It is also necessary for the narrow pulse approximation to be valid. If it is not, $\phi(q\Delta)$ still has a linear region, but the slope is no longer $\langle V \rangle$ and the measurements can be easily misinterpreted.

We have also been able to measure the averaged propagator in porous systems. These measurements can be interpreted as velocity distributions if a time average velocity is defined. $n(\bar{v};\Delta)$ is profoundly dependent on the observation time. $n(\bar{v};\Delta)$ approximates the instantaneous velocity spectrum only within a limited range of observation times. For water flowing in typical rock cores, this range is probably incompatible with reservoir flow rates and typical NMR instrumentation. However, if a more viscous fluid is used, an approximation of the instantaneous velocity spectrum might still be obtained. The dependence of $n(\bar{v};\Delta)$ on observation time also presents an opportunity. Using a judicious choice of Δ, it will be easy to estimate the flowing and nonflowing fractions of fluid.

Finally the shape of $n(\bar{v};\Delta)$ does not necessarily reflect aspects of pore space geometry. One cannot conclude that a uniform pore structure exists simply because $n(\bar{v};\Delta)$ is a narrow symmetric peak about $\langle V \rangle$. This may also be an indication that a long observation time has been used and significant velocity averaging has occurred.

REFERENCES

1. M.A. Robinson, "Application of MRI to Porous Media: Correlation Between Porosity and Average Flow Velocity During Displacement Experiments," *33rd Experimental Nuclear Magnetic Resonance Conference*, poster WP 171, Pacific Grove, March 1992.

2. M.A. Robinson, and W.A. Edelstein, "Fluid Velocities in Oil Cores During Water Injections," *1991 SCA Annual Technical Conference*, Paper#9113, San Antonio, August 1991.

3. M.A. Robinson, "Measurement of Fluid Velocities During Water Injection Into Natural Porous Rocks," SPE 24369, 1992.

4. P. Mansfield, and B. Issa, "Studies of Fluid Transport in Porous Rocks by Echo-Planar MRI," *Second International Metting on Recent Advances in Magnetic Resonance Applications to Porous Media* Canterbury, United Kingdom, April 1993.

5. C.T. Chang, and C.M. Edwards, "Velocity Measurements of Fluid Flow in Porous Media Using NMR Imaging," *Annual APS Condensed Matter Division Conference*, March 1993.

6. P. Mansfield, R. Bowtell, S. Blackband, and D.N. Guifoyle, "Magnetic Resonance Imaging: Applications of Novel Methods in Studies of Porous Media," *Mag. Res. Imag.* **10**, 741(92).

7. A.T. Watson, private communication.

8. A. Caprihan, R.H. Griffy, and E. Fukushima, "Velocity Imaging Slow Coherent Flows Using Stimulated Echoes," *Mag. Res. Med.* **15**, 327(90).

9. P. T. Callaghan, Principles of Nuclear Magnetic Resonance Microscopy, Clarendon Press, Oxford, 1991.

10. Q.S. Xiang, and O. Nalcioglu, "Measurement of Mean and Variance of Velocity Fields Within Each Voxel by NMR Imaging," *IEEE Trans. on Med. Imag.* **7**, 364(88).

11. J. Bear, Dynamics of Fluids in Porous Media, Academic Press, New York, 1975.

12. D. Herrick, private communication.

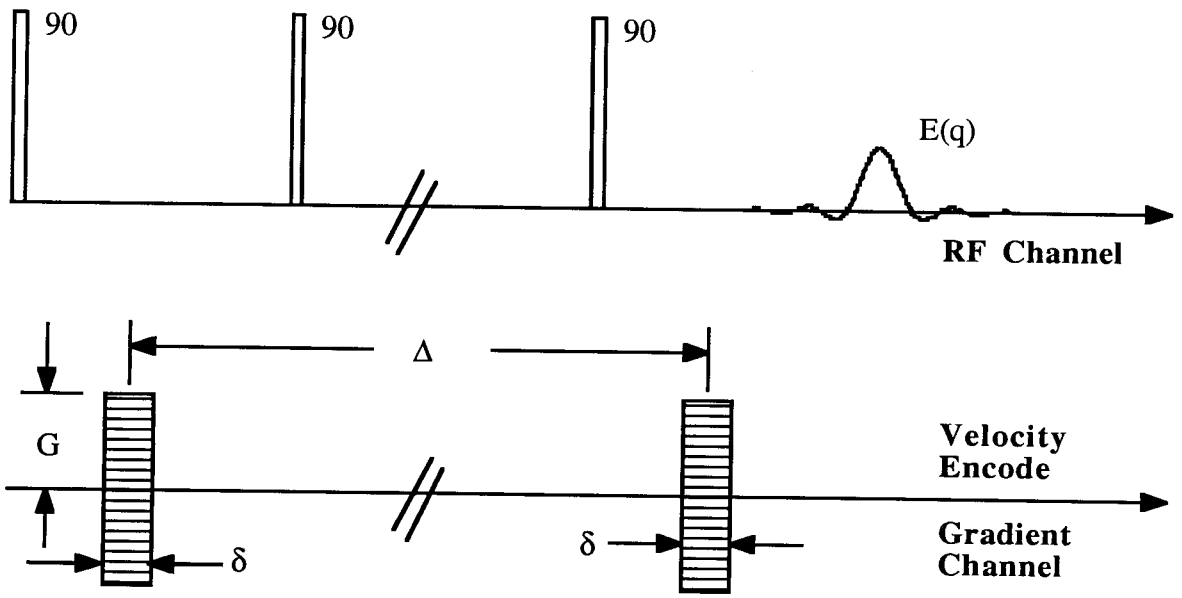

Fig. 1: Velocity encoding portion of a typical stimulated echo imaging pulse sequence. The position encoding segments of the sequence are not shown. Positioning encoding is performed in the usual way. Velocity encode gradient has a range of values to measure velocity distributions but only a single value to measure ⟨V⟩.

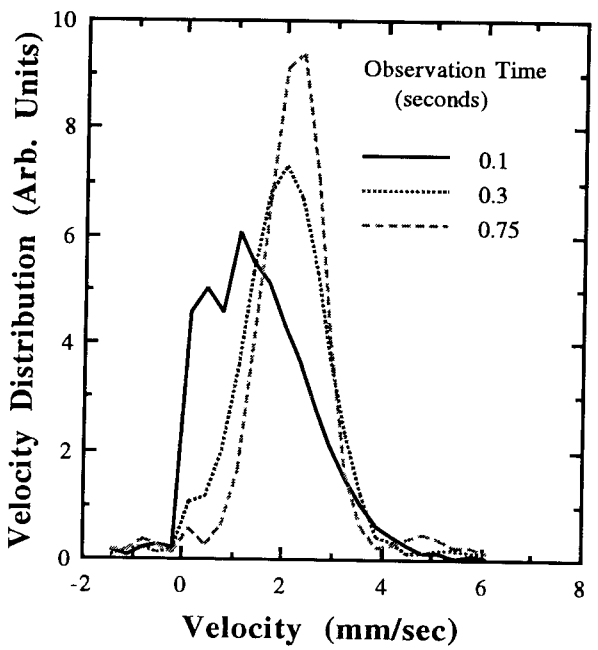

Fig. 2: Velocity distribution for water flow in 0.2 mm glass bead pack at different observation times. The flow rate equals 16 ml/min.

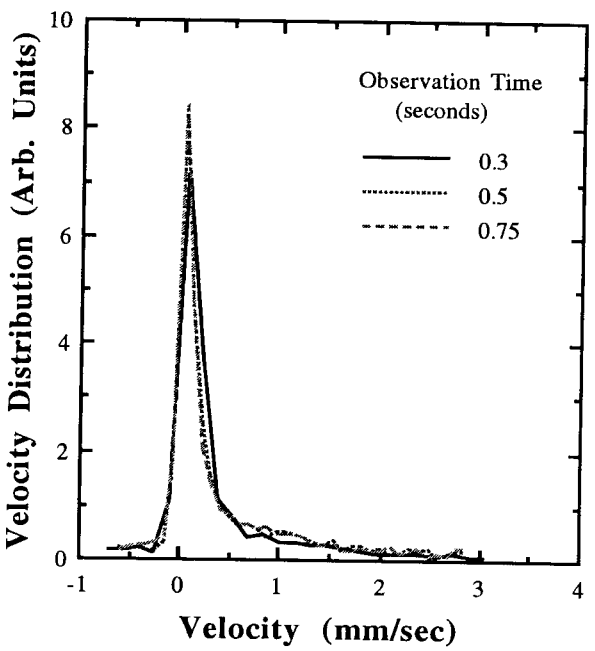

Fig. 3: Velocity distribution for water flow in Bentheim sandstone at different observation times. The flow rate equals 4.8 ml/min.

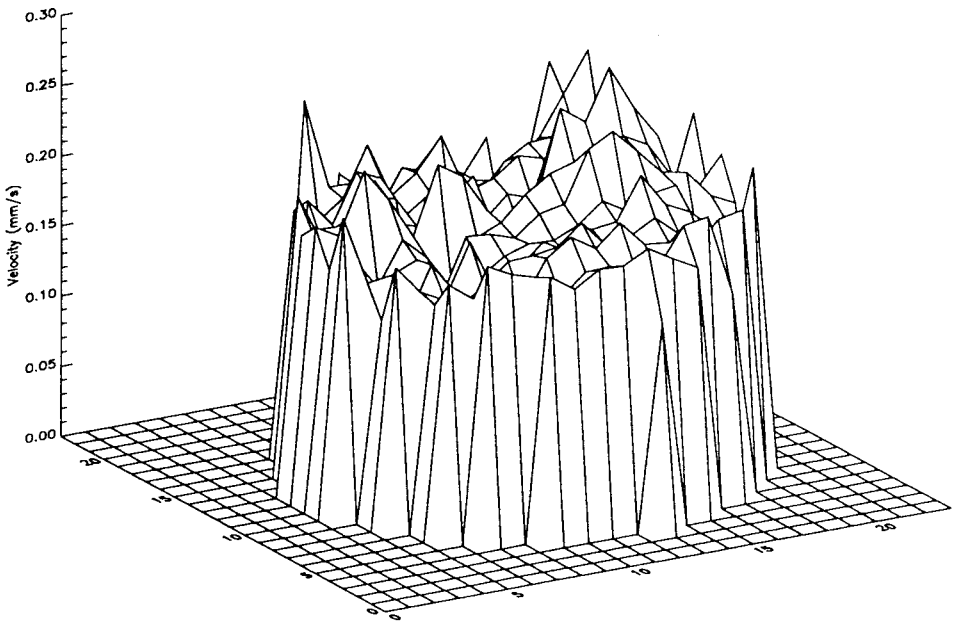

Fig. 4: Average velocity image for 0.2 mm bead pack. Flow rate equals 16 ml/min. The values of velocity in this image are in good agreement with the Dupuit-Forchheimer velocity.

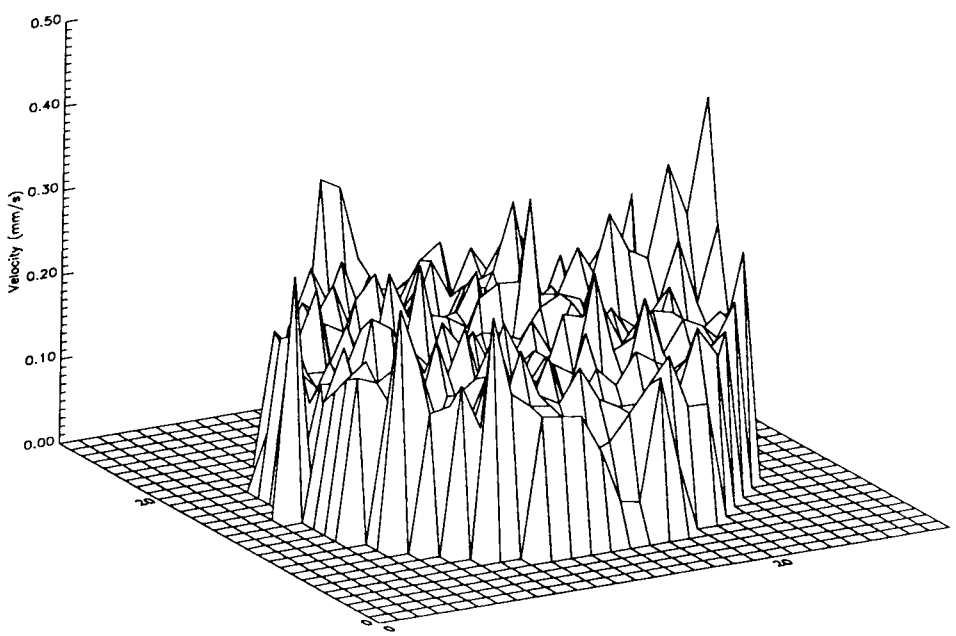

Fig. 5: Average velocity image for Bentheim sandstone. Flow rate equals 4.8 ml/min. The values of velocity in this image are 30% lower than the Dupuit-Forchheimer velocity.

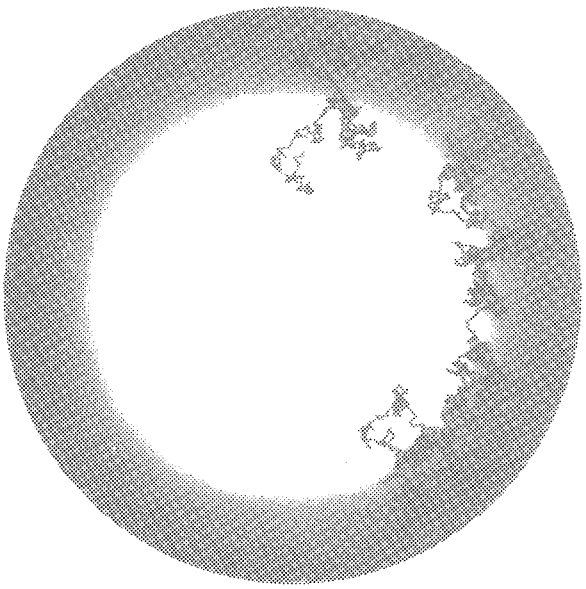

Fig. 6: Typical path of a molecule diffusing in a capillary tube. The line represents the projection of its path on a plane perpendicular to the symmetry axis of the capillary tube. The gray back represents the velocity field of the fluid moving by laminar flow down the capillary. Dark to light represents increasing velocity. The radius of the tube is 45 μm and the observation is approximately 0.5 seconds.

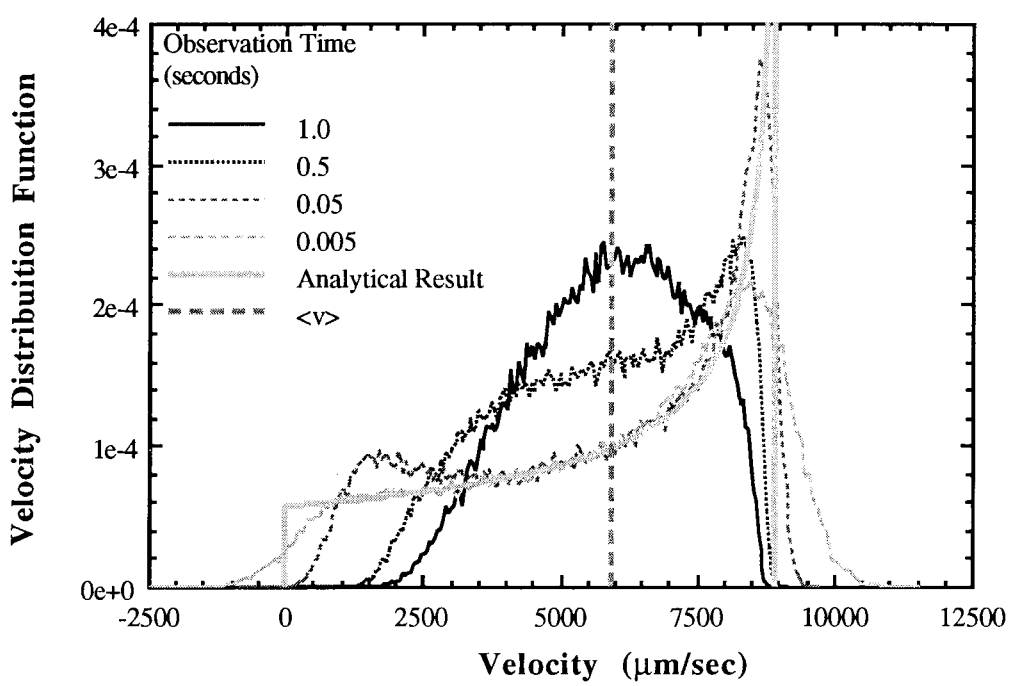

Fig. 7: Velocity distribution calculated from a random walk simulation of water flow between parallel flat plates. v_m is 8.9 mm/sec. Distance between the plates is 90 μm. $a^2/2D = 0.5$ sec. and $2D/v_m^2 = 50$ μsec.

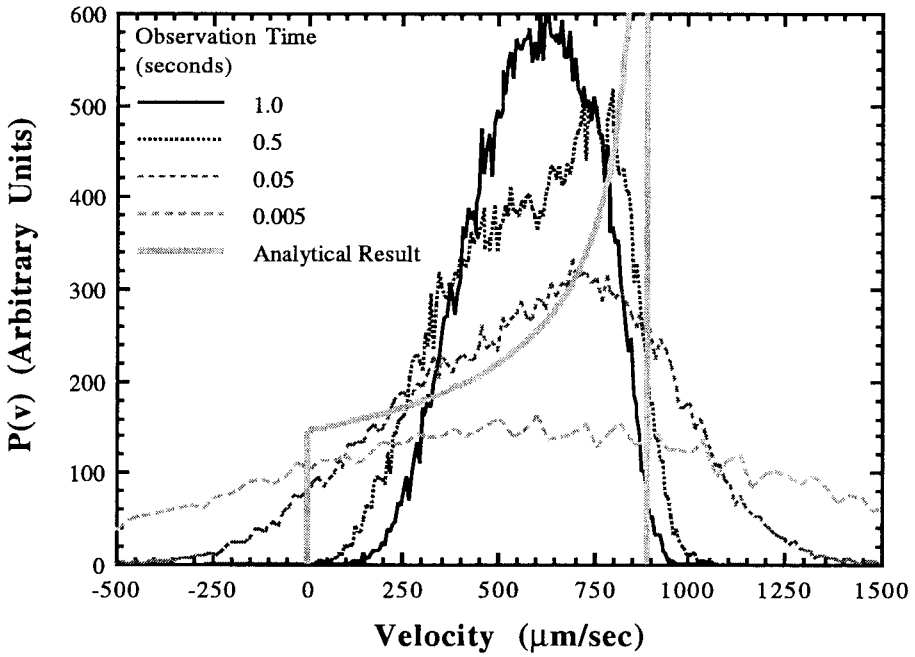

Fig. 8: Velocity distribution calculated from a random walk simulation of water flow between parallel flat plates. v_m is 0.89 mm/sec. Distance between the plates in 90 μm. $a^2/2D = 0.5$ sec. and $2D/v_m^2 = 5$ msec.

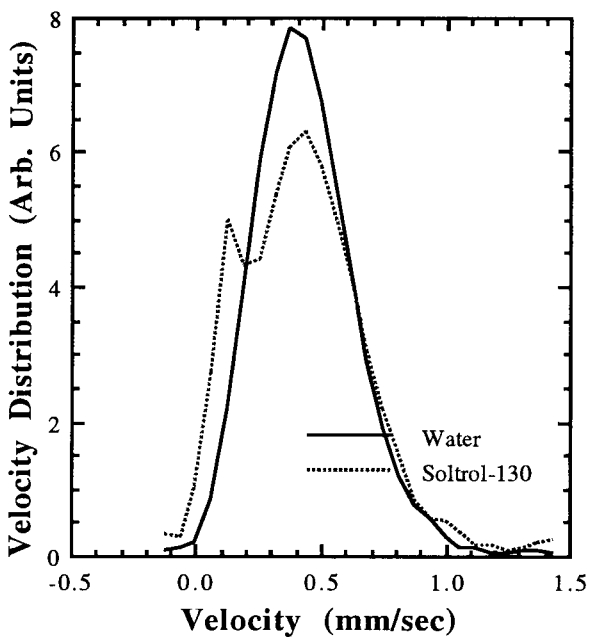

Fig. 9: A comparison of velocity distribution for water and Soltrol-130 flowing through the 0.2 mm beadpack at a flow rate of 5 ml/min. The observation time was 0.5 seconds.

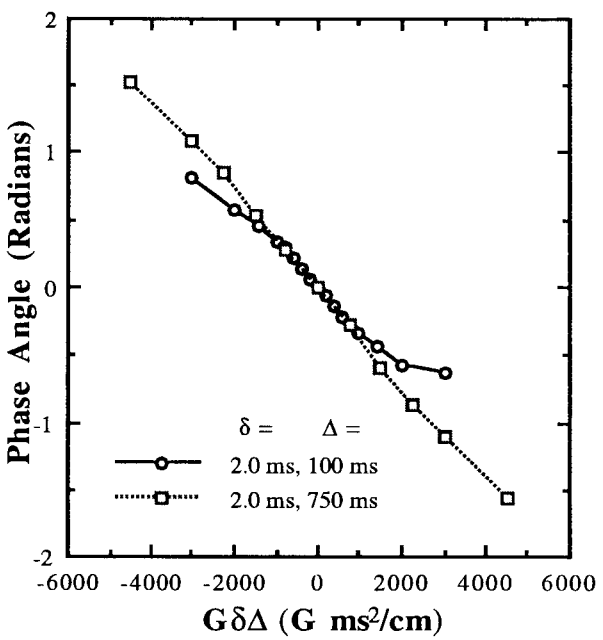

Fig. 10: The phase shift from a voxel for water flow at 1.6 ml/min in the 0.2 mm beadpack. The linear regime is wider for the data with longer observation time.

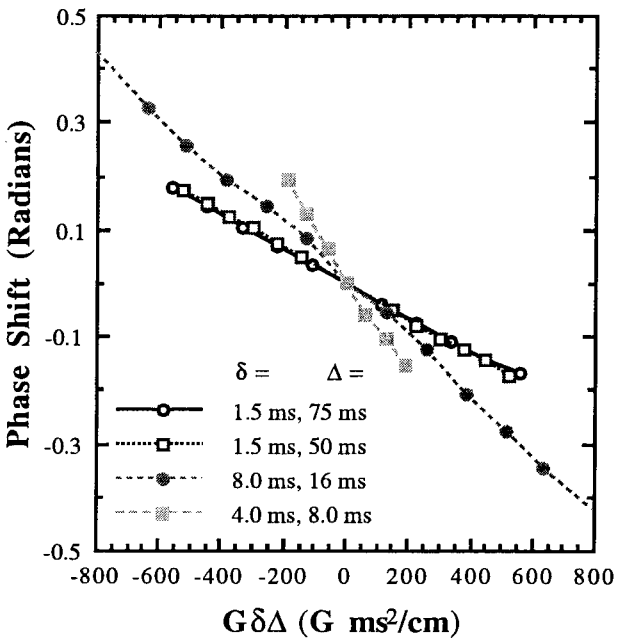

Fig. 11: The phase shift for water flow (2 ml/min) in the Bentheim Sample. Note the difference between the narrow pulse and finite pulse conditions.

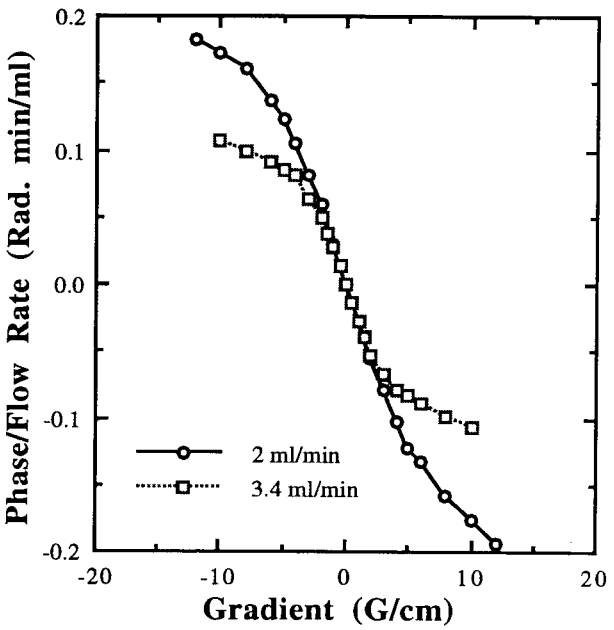

Fig. 12: Phase angle as a function of gradient strength normalized by the flow rate. The narrow pulse conditions was satisfied in these measurements.

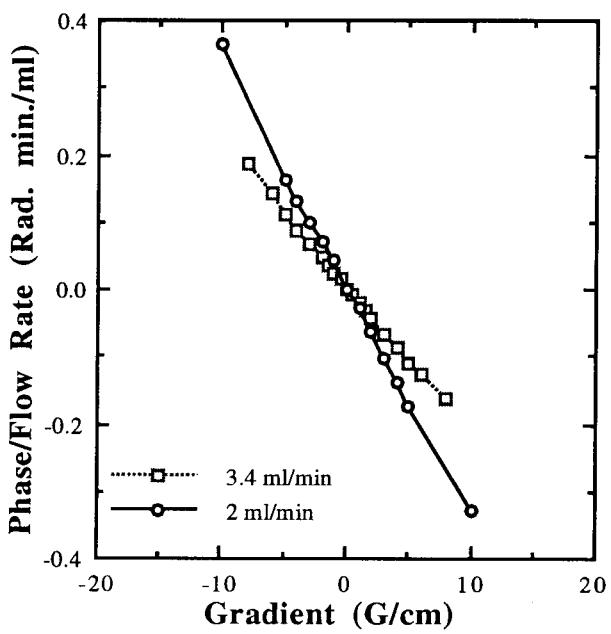

Fig. 13: Phase angle as a function of gradient strength, normalized by flow rate for water flow in Bentheim sandstone. In these sets of data, the narrow pulse approximation is not valid and the slope of the line is not ⟨V⟩.